SUPPLEMENTARY INFORMATION

Structural Evidence for Product Stabilization by the Ribosomal mRNA Helicase

Hossein Amiri[a] and Harry F. Noller[b]

Center for Molecular Biology of RNA and Department of Molecular, Cell and Developmental Biology, University of California at Santa Cruz
Santa Cruz, CA 95064, USA

[a]Present Address: Department of Molecular and Cell Biology, University of California at Berkeley, Berkeley, CA 94720, USA

[b]To whom correspondence should be addressed. Email: harry@nuvolari.ucsc.edu

SUPPLEMENTARY FIGURES

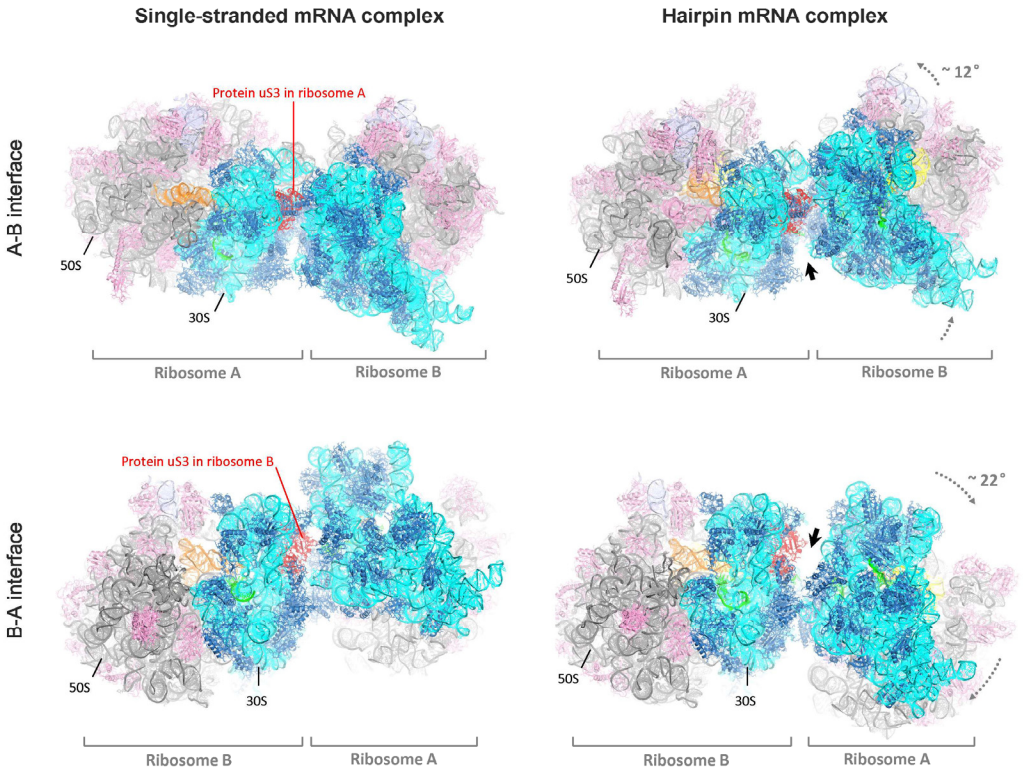

Supplementary Figure S1. Crystal packing rearrangement in the presence of mRNA hairpin. The crystal packing of ribosomes in the hairpin mRNA complex (right column; this study) is compared to that for the classical/hybrid-state complex with unstructured single-stranded mRNA (left column; PDB 4V9D) (Dunkle et al. 2011), when aligned on 16S rRNA of either ribosome A (top row) or ribosome B (bottom row). Note that as a result of the rigid-body movement of ribosomes A and B relative to each other in the hairpin complex, more space has become available in front of protein uS3 (red) in the expected locations of the mRNA hairpin, as indicated by thick arrows.

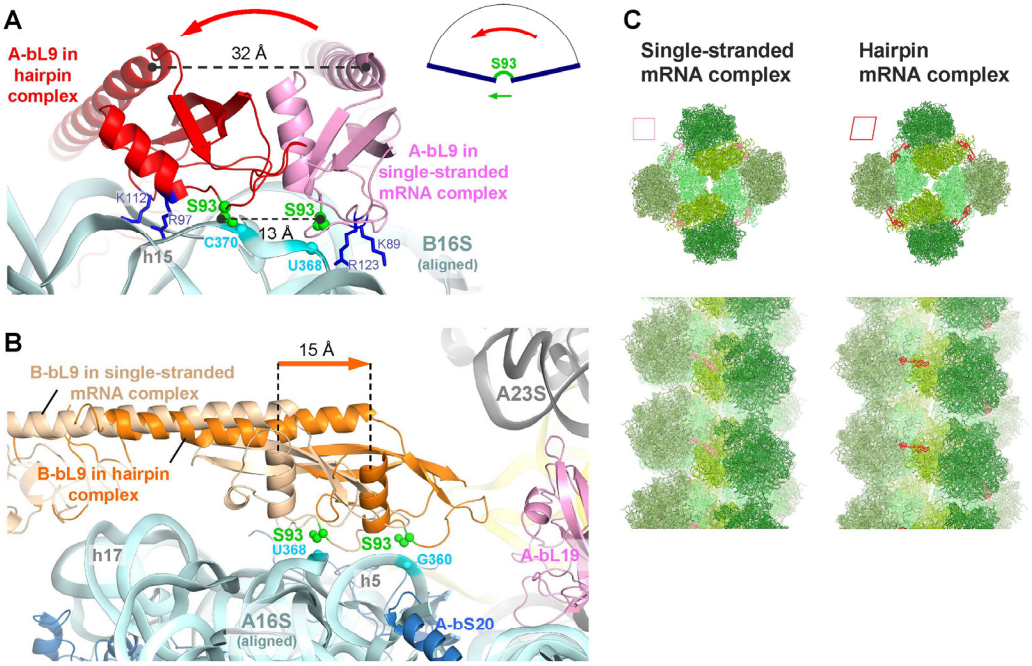

Supplementary Figure S2. Remodeling of crystal contacts of ribosomal protein L9 in the presence of mRNA hairpin. (A) The globular C-terminal domain of protein bL9 in its classical position (pink) contacts helix h5 and the base of helix h15 of the neighboring 16S rRNA. In particular, Ser93 of bL9 (green) contacts the backbone phosphate of U368 (cyan) in helix h15, and Phe91 packs on the bulged A55 in helix h5 (shown in Figure 1D). The bL9 protein in ribosome A (red) is shifted from its classical position by about 30 Å at its α helical joint, forming a new binding interface on the opposite side of Ser93 on helix h15 of 16S rRNA, involving Arg97 and Lys112 (blue). In turn, most of the classical-state interface between Lys89 and Arg123 (also blue) is now lost. The two bL9 conformations are related by a sliding pivot motion, as indicated on the right. (B) The bL9 protein in ribosome B (orange) is moved by ~15 Å toward the body of the neighboring 16S rRNA compared to the classical position (light orange), such that Ser93 (green) interacts with the phosphate of G360 (cyan). (C) Comparison between the ribosome packing profiles calculated from a crystal structure with unstructured mRNA (left; PDB 4V9D) (Dunkle et al. 2011) and the hairpin complex (right). The top view (top), normal to the a-axis, shows the position of the bL9 protein (pink or red) in the polysome-like helical array. The small and large subunits of the A and B molecules are in different shades of green. Note the appearance of the X-shaped white space in the center of the array in the hairpin complex, corresponding to the extra room between neighboring ribosomes to accommodate the hairpin. The side view of the polysome helical array for each of the structures (bottom), where the a-axis runs vertically, shows changes in the relative orientation of the neighboring ribosomes.

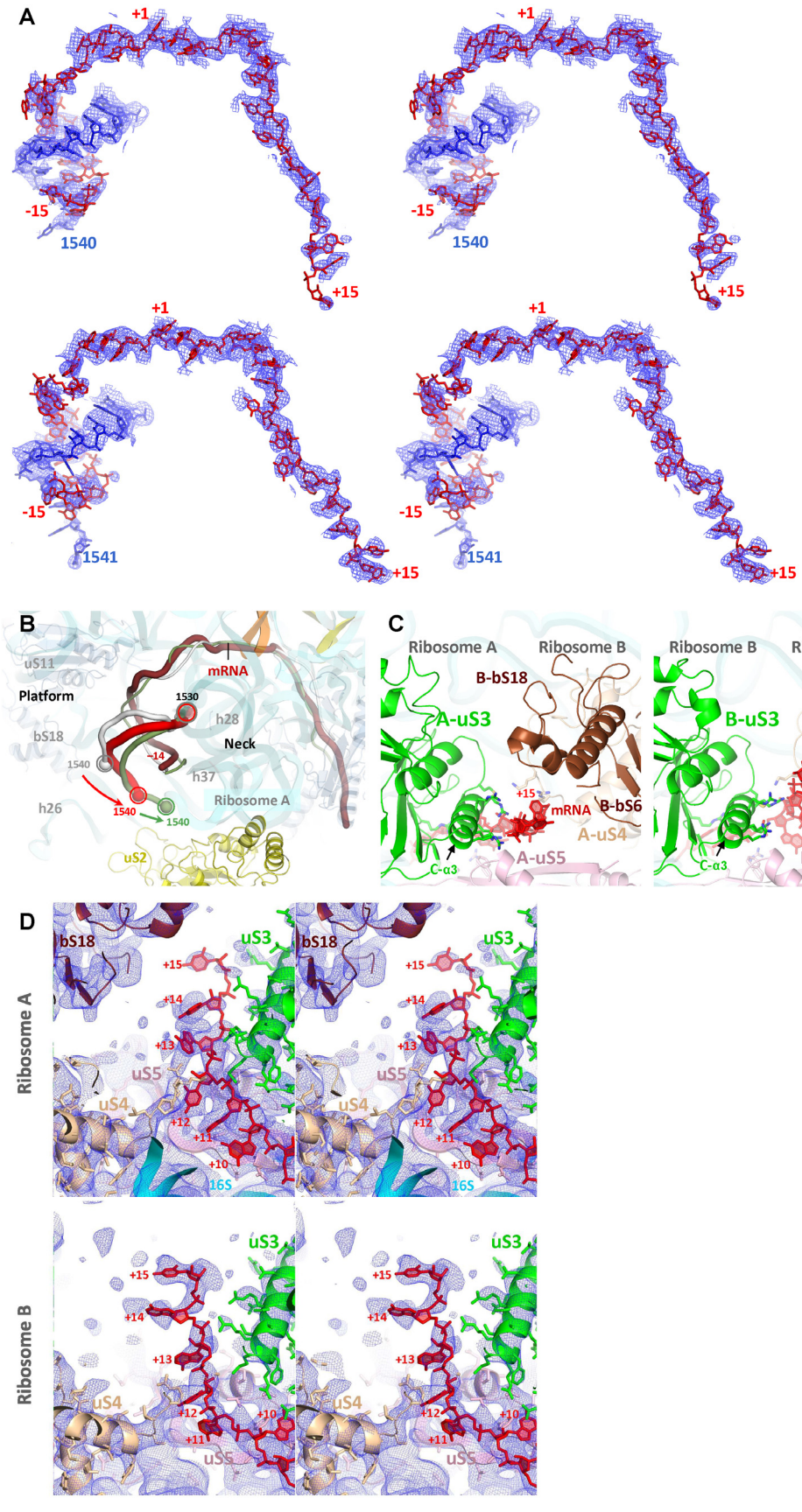
A
+1
-15
1540
+15
+1
-15
1540
+15
+1
-15
1541
+15
+1
-15
1541
+15
B
uS11
mRNA
Platform
1530
h28
bS18
Neck
-14
1540
h37
h26
1540
1540
Ribosome A
uS2
C
Ribosome A
Ribosome B
B-bS18
A-uS3
+15
mRNA
B-bS6
A-uS4
A-uS5
C-α3
Ribosome B
Ribosome A
A-uS11
B-uS3
+15
mRNA
B-uS4
B-uS5
C-α3
D
Ribosome A
bS18
uS3
+15
+14
+13
uS5
uS4
+12
+11
+10
16S
Ribosome B
uS3
+15
+14
+13
uS4
+12
+10
+11
uS5

Supplementary Figure S3. Structure of the mRNA in the hairpin complex. (A) Stereo view of the mRNA model (red) and 2mFo-DFc electron density map contoured at 0.8σ (blue) in ribosome A (top) and ribosome B (bottom). The anti-SD sequence from the 16S rRNA is shown in light blue. (B) The orientation of the SD helix in the hairpin complex (red) is closer to that of the posit-initiation complex (green, PDB 4V4Y) than the initiation complex (white, PDB 4V4Z) (Yusupova et al. 2006), and points toward protein uS2 in the neck region. Nucleotides 1530 and 1540 which are near the two ends of the SD helix are circled. (C) Crowding outside of the tunnel in ribosomes A and B as viewed from the 30S head domain. Proteins bS6 and bS18 (brown) from the symmetry mate approach the tunnel entrance in ribosome A. In contrast, the space in front of the entrance in ribosome B is much less crowded. (D) Stereo views of the mRNA (red) interacting with protein S3 (green) at the tunnel entrance, and 2mFo-DFc electron density map (blue) contoured at 1σ for ribosome A (top panels) and B (bottom panels), showing the extent of background noise.

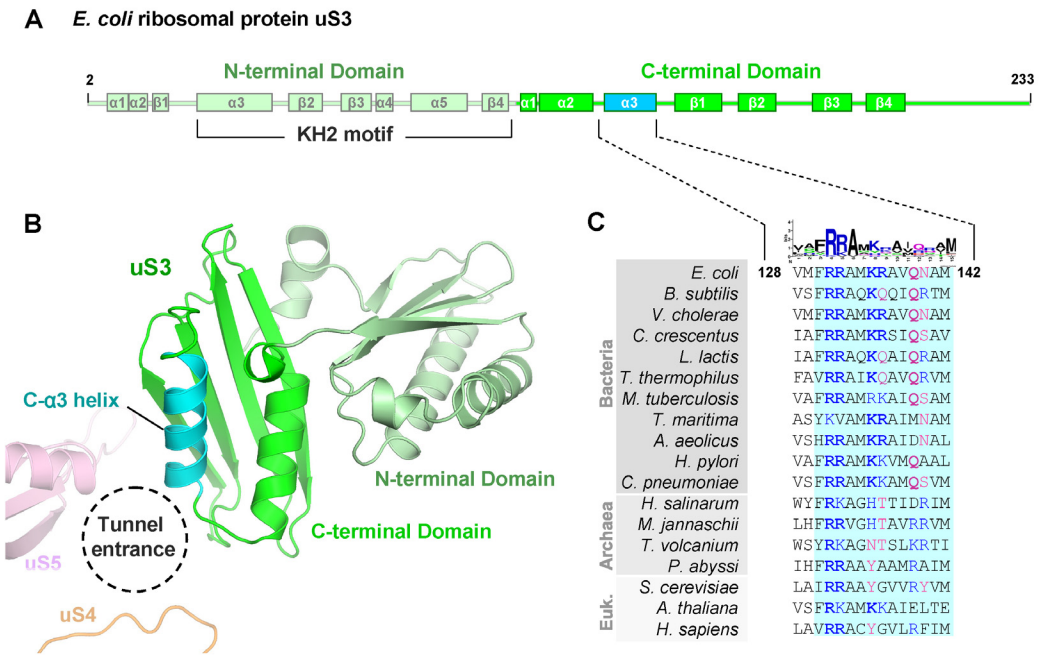

Supplementary Figure S4. Architecture of *E. coli* ribosomal protein uS3. (A) uS3 is composed of two major globular domains: an N-terminal domain (faint green) with α/β fold, which includes the type II protein K homology (KH2) domain, and a C-terminal domain (bright green) with an α+β fold, in which the third α helix (C-α3) is indicated in cyan. (B) The C-α3 helix is in the vicinity of the mRNA tunnel entrance in the ribosome. (C) The C-α3 helix is conserved across the three domains of life. Arg131 and Arg132 are almost universally conserved, while Lys135 and Arg136 are mostly conserved in bacteria.

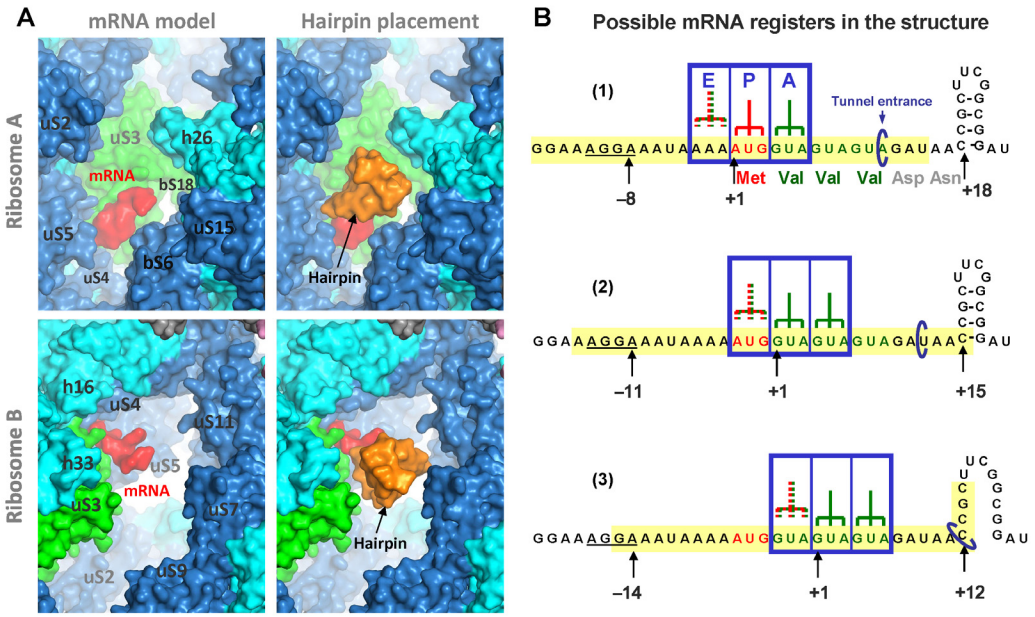

Supplementary Figure S5. Inferred location of the hairpin in the structure. (A) In the left images, the observed segments of mRNA (red) up to position +15 in ribosome A (top) and ribosome B (bottom) approach cavities between adjacent ribosomes, and are bound to protein uS3 (green). Note that, for clarity, the views for ribosomes A and B are from different angles. The right images show that the cavities are large enough to house a putative hairpin (orange) starting at position +15 on each mRNA. Other placements of the hairpin (e.g. at +18; not shown) are also possible for each mRNA. (B) Three possible positions of the ribosome (blue box with A, P, and E sites indicated) on the mRNA are shown schematically for the crystal structure. With only fMet and Val tRNAs present, these are the only positions that would allow cognate or near-cognate tRNA-mRNA base-pairing in both A and P sites, as seen in the structure (see Figure 5 and Supplementary Figure S6C,D). The positions of the SD sequence and the hairpin relative to the first nucleotide of the P site codon (+1) are indicated for each possibility. The region of mRNA seen in the crystal structure (from –15 to +15) is highlighted in yellow. The second possibility (2) is the most likely based on the structure. The first possibility corresponds to an initiation complex, which is not supported by the observed orientation of the SD helix (Supplementary Figure S3B). The third possibility also seems less likely, because the observation of single-stranded mRNA from position +12 to +15 would require unwinding of the hairpin. We cannot rigorously exclude any of these possibilities, one or more of which may be represented in the crystal.

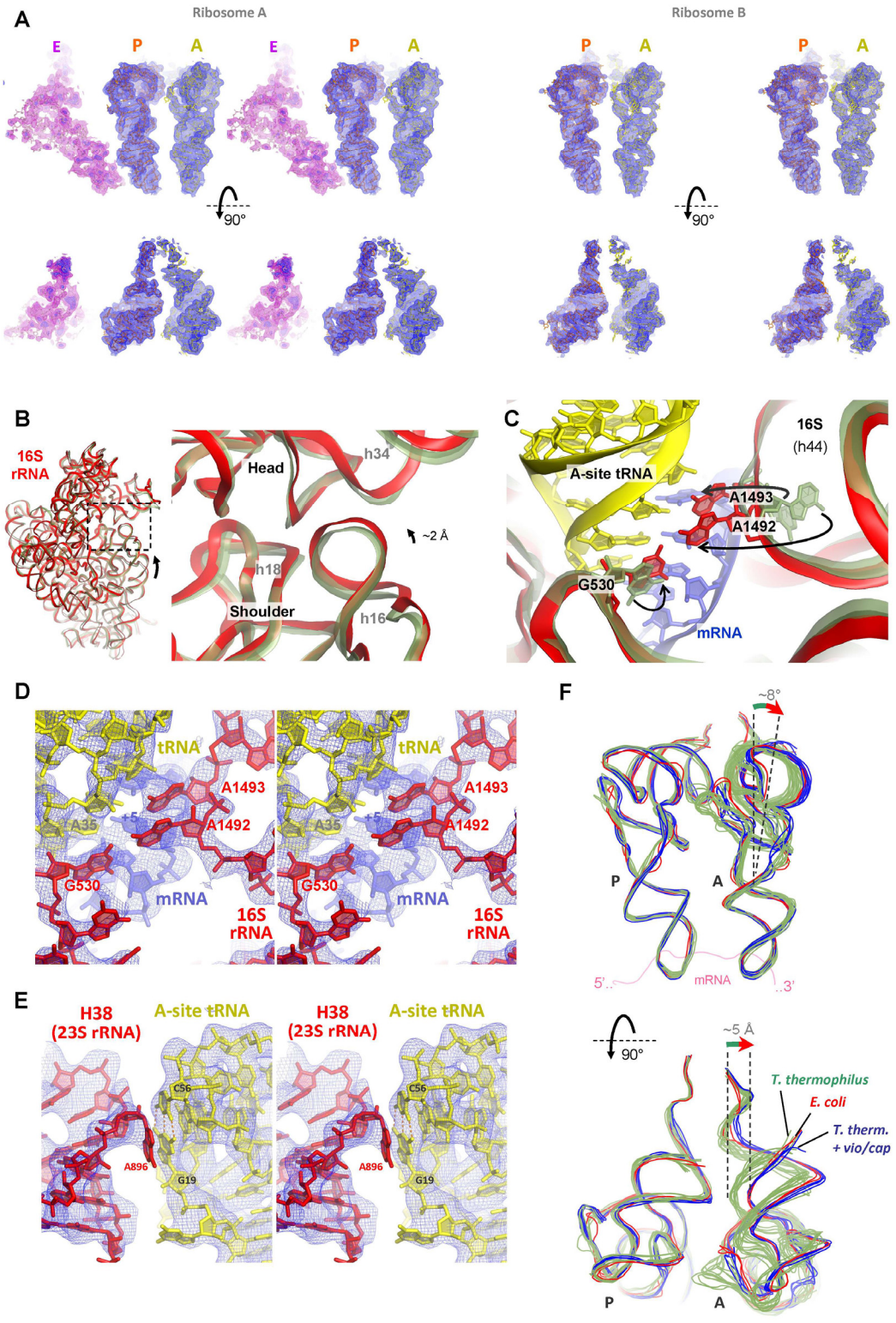
A
Ribosome A
Ribosome B
E
P
A
90°
B
16S rRNA
Head
h34
~2 Å
h18
Shoulder
h16
C
16S (h44)
A-site tRNA
A1493
A1492
G530
mRNA
D
tRNA
A1493
A1492
A35
+5
G530
mRNA
16S rRNA
E
H38 (23S rRNA)
A-site tRNA
C56
A896
G19
F
~8°
P
A
5'
mRNA
3'
~5 Å
T. thermophilus
E. coli
T. therm. + vio/cap

Supplementary Figure S6. Features of A-site tRNA binding in the hairpin complex. (A) Stereo views of 2mFo-DFc map for the tRNAs in ribosome A (left) and B (right) as viewed from the subunit interface (top row) or from the large subunit (bottom row), contoured at 1σ (blue) for A- and P-site tRNAs and at 0.3σ (purple) for the E-site tRNA. (B) Comparison of 30S domain conformation in the hairpin complex structure (red) with the classical/hybrid-state complex with unstructured mRNA (green, PDB 4V9D) (Dunkle et al. 2011), after alignment of protein uS3 of ribosome B in each structure. (C) Comparison of the arrangement in decoding center between the two structures in panel B, showing the flipping of the 16S nucleotides A1492 and A1493 toward the tRNA-mRNA base pairs (in yellow and blue, respectively), and flipping of the G530 base into the *anti* conformation. (D) Stereo view of the decoding center in the hairpin complex, and the 2mFo-DFc map (blue) contoured at 1.5σ and sharpened by 60Å^2. (E) Stereo view of H38 helix of 23S rRNA (finger helix, red) interaction with the elbow of A-site tRNA (yellow), and the 2mFo-DFc map (blue) contoured at 0.8σ. (F) Backbone traces of A- and P-site tRNAs in the *E. coli* hairpin complex (red, this study), *T. thermophilus* complexes with peptide antibiotics viomycin or capreomycin (blue, PDB 4V7L and 4V7M) (Stanley et al. 2010), and *T. thermophilus* complexes with paromomycin or no antibiotic (green, PDB 4V5C, 4V5D, 4V6F, 4WT1, 5IBB, 5E7K, and 5IB7) (Jenner et al. 2010; Rozov et al. 2015, 2016a, 2016b; Voorhees et al. 2009), after alignment of all structures with respect to the 23S rRNA. Whereas the P-site tRNA is superimposable in all of the complexes, view from the subunit interface (top) shows that the A-site tRNA in the first two categories (red and blue) is bent such that its acceptor and T arms are further away from those of the P-site tRNA. Top view from the large subunit (bottom) shows that the A-site tRNA backbone in the first two categories (red and blue) follows a distinct path that widens the gap between the A- and P-site tRNAs by ~5Å in the acceptor arm region. Note that tRNAs from two ribosomes in the asymmetric unit are represented for each structure.

SUPPLEMENTARY TABLE

Name (type)	Use	Sequence [a]
pH03H9 (mRNA)	Crystallization (Hairpin complex)	GGAAAGGAAAUAAAAAUGGUAGU AGUAGAUAACCGCUUCGGCGGAU
fMVVV (mRNA)	Toeprinting assay, filter binding assay	GGAAAGGAAAUAAAAAUGGUAGU AGUAGAUAGAAAAUAAUAGAAGA AUCGGAUAAGAGAACACAGGAUC CAG
TP2 (DNA oligonucleotide)	Toeprinting assay	CTGGATCCTGTGTTCTC

[a] The SD motif, start codon, and hairpin sequence are underlined.

Supplementary Table S1. Nucleic acid sequences used in this study

SUPPLEMENTARY REFERENCES

Dunkle JA, Wang L, Feldman MB, Pulk A, Chen VB, Kapral GJ, Noeske J, Richardson JS, Blanchard SC, Cate JHD. 2011. Structures of the bacterial ribosome in classical and hybrid states of tRNA binding. *Science* **332**: 981–984.

Jenner LB, Demeshkina N, Yusupova G, Yusupov M. 2010. Structural aspects of messenger RNA reading frame maintenance by the ribosome. *Nat Struct Mol Biol* **17**: 555–560.

Rozov A, Demeshkina N, Khusainov I, Westhof E, Yusupov M, Yusupova G. 2016a. Novel base-pairing interactions at the tRNA wobble position crucial for accurate reading of the genetic code. *Nat Commun* **7**: 10457.

Rozov A, Demeshkina N, Westhof E, Yusupov M, Yusupova G. 2015. Structural insights into the translational infidelity mechanism. *Nat Commun* **6**: 7251.

Rozov A, Westhof E, Yusupov M, Yusupova G. 2016b. The ribosome prohibits the G•U wobble geometry at the first position of the codon-anticodon helix. *Nucleic Acids Res* **44**: 6434–6441.

Stanley RE, Blaha G, Grodzicki RL, Strickler MD, Steitz TA. 2010. The structures of the anti-tuberculosis antibiotics viomycin and capreomycin bound to the 70S ribosome. *Nat Struct Mol Biol* **17**: 289–293.

Voorhees RM, Weixlbaumer A, Loakes D, Kelley AC, Ramakrishnan V. 2009. Insights into substrate stabilization from snapshots of the peptidyl transferase center of the intact 70S ribosome. *Nat Struct Mol Biol* **16**: 528–533.

Yusupova G, Jenner L, Rees B, Moras D, Yusupov M. 2006. Structural basis for messenger RNA movement on the ribosome. *Nature* **444**: 391–394.